



Title	Quantitative Observation of Electric Potential Distribution of Brittle Polyelectrolyte Hydrogels Using Microelectrode Technique
Author(s)	Guo, Honglei; Kurokawa, Takayuki; Takahata, Masakazu; Hong, Wei; Katsuyama, Yoshinori; Luo, Feng; Ahmed, Jamil; Nakajima, Tasuku; Nonoyama, Takayuki; Gong, Jian Ping
Citation	Macromolecules, 49(8), 3100-3108 https://doi.org/10.1021/acs.macromol.6b00037
Issue Date	2016-04-26
Doc URL	http://hdl.handle.net/2115/64953
Rights	This document is the Accepted Manuscript version of a Published Work that appeared in final form in Macromolecules, copyright ©2016 American Chemical Society after peer review and technical editing by the publisher. To access the final edited and published work see http://pubs.acs.org/doi/pdf/10.1021/acs.macromol.6b00037
Type	article (author version)
Additional Information	There are other files related to this item in HUSCAP. Check the above URL.
File Information	Manuscript-10th-20160322 for university.pdf (Main Text)



[Instructions for use](#)

Quantitative observation of electric potential distribution of brittle polyelectrolyte hydrogels using microelectrode technique

Honglei GUO¹, Takayuki KUROKAWA^{2,3}, Masakazu TAKAHATA⁴, Wei HONG^{3,5}, Yoshinori
KATSUYAMA², Feng LUO², Jamil AHMED¹, Tasuku NAKAJIMA^{2,3}, Takayuki NONOYAMA^{2,3},
Jian Ping GONG*^{2,3}

¹Graduate School of Life Science, Hokkaido University, Sapporo, 060-0810, Japan

²Faculty of Advanced Life Science, Hokkaido University, Sapporo, 060-0810, Japan

³Global Station for Soft Matter, Global Institution for Collaborative Research and
Education, Hokkaido University, Sapporo, 060-0810, Japan

⁴Faculty of Science, Hokkaido University, Sapporo, 060-0810, Japan

⁵Department of Aerospace Engineering, Iowa State University, Ames, IA 50011, USA

*Corresponding author

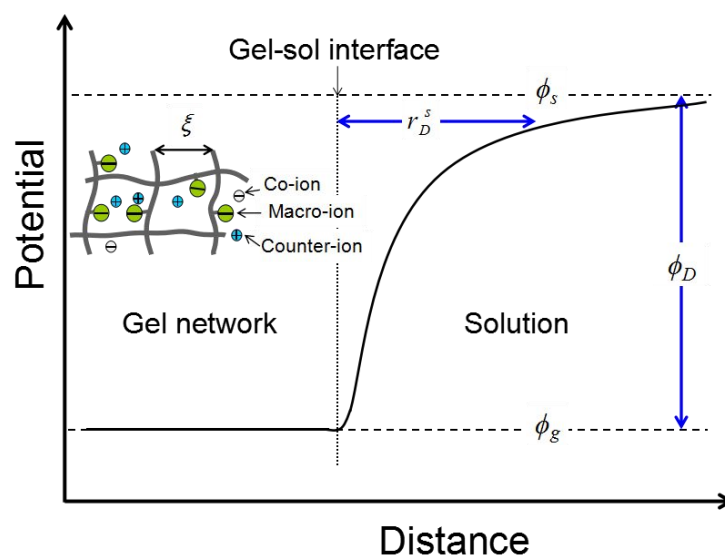
Tel/Fax: +81-11-706-2774, E-mail: gong@mail.sci.hokudai.ac.jp

Abstract:

We report, for the first time, the quantitative measurement of the local electric potential of brittle polyelectrolyte hydrogels using the microelectrode technique (MET). Given the solid-like nature of the hydrogels, the difficulty of applying MET is how to make a good contact of the microelectrode to the hydrogel. Poor local contact substantially underestimates the potential. We observed that, the potential measured decays exponentially with the increase of capillary diameter of the microelectrode. This behavior is related to the capillary wall thickness that determines the contact distance of the electrode probe to the hydrogel. The characteristic decay length in respect to the wall thickness was very close to the local Debye length around the capillary. The latter is much larger than that of the bath solution due to the reverse osmosis effect. By using microelectrodes with a tip wall thickness less than the local Debye length, the Donnan potential of polyelectrolyte gel could be accurately measured. Using a micromanipulator, the inserting process of the microelectrode is precisely controlled, and the depth profile of electric potential in the hydrogels can be measured with a spatial resolution down to ~ 5 nm. From the spatial distribution of potential, the micro-structure of hydrogels both in bulk and near the surface, the thickness of ultra-thin hydrogels, and the heterogeneous layered structure of composite gels, can be determined accurately. The MET established in this work provides a powerful tool for direct characterization of the spatial distribution of electric potential of hydrogels.

Introduction

Polyelectrolytes are polymers carrying ionic and/or ionizable groups. Compared with neutral hydrogels, polyelectrolyte hydrogels have many unique properties, such as high water-absorbing capacity¹, ion exchange ability², ionic conductivity³, ion-strength sensitivity⁴, mechano-electrical effect⁵, and very low surface friction⁶. Some of these properties are responsible for the functionalities of articular cartilage⁷, double network hydrogels⁸, electrochemical fuel cells⁹, drug release control¹⁰, etc.



Scheme 1. Electric potential of a polyelectrolyte hydrogel carrying negative macro-ions. The polyelectrolyte network carries macro ions that are immobilized on the 3-D network, and small counter ions and co-ions that are movable. Inside the gel, there is potential variation over the mesh size ξ of the network. For a homogeneously crosslinked gel, the potential of the gel is constant at the micrometer scale. On the surface of the gel, an electric double layer is formed, and there exists a large potential difference between the polyelectrolyte hydrogel and surrounding bath solution. At thermodynamically equilibrium state, the latter is the Donnan potential $\phi_D = \phi_g - \phi_s$, where ϕ_g and ϕ_s are potential of the gel and the bath solution, respectively. r_D^s is the Debye

length of the bath solution.

The spatial distribution of electric potential reveals important structural information of polyelectrolyte hydrogels. A polyelectrolyte hydrogel is loaded with macro ions that are fixed on the 3-D polymer network as well as small ions that are mobile in the aqueous solution. The mobile ions carrying the same type of charge as the fixed ions are often referred to as the co-ions, while those carrying opposite charge are called counter-ions. Both two types of mobile ions are present in a polyelectrolyte gel. Deep inside the gel, there is potential variation in nano-scale over the mesh size ξ of the network. When observed at a scale much larger than the mesh size, the potential is constant for a homogeneous hydrogel. Heterogeneous distribution of fixed macro ions will lead to spatial modulation of potential.

There is a large potential difference, known as the Donnan potential, between the gel and the bath solution. When a concentration difference is present between the gel and the solution, the mobile ions tend to migrate across gel-solution interface under the entropic driving force. The electrostatic interaction from the fixed ions, on the other hand, attracts the counter ions and repels the co-ions. While it is still electrically neutral deep inside the gel and in the solution, the competition between electrostatic interaction and ionic diffusion would result in an electric double layer at the interface. The Donnan potential is a direct consequence of the interfacial double layer at thermodynamically equilibrium state, i.e. the Donnan equilibrium¹¹. The Donnan equilibrium often generates a large ionic osmotic pressure which substantially swells

polyelectrolyte gels in water and low ionic strength solutions.

From the electrochemical equilibrium condition, the Donnan potential is related to the activity of mobile ions in the gel, a_{ion}^g and that in the bath solution a_{ion}^s .¹¹

$$\phi_D = \phi_g - \phi_s = \frac{2.3RT}{zF} \log \frac{a_{ion}^s}{a_{ion}^g} \quad (1)$$

Here, where ϕ_g and ϕ_s are potential of the gel and the bath solution, respectively, z is the valence of the mobile ion in consideration, R is the gas constant, T is the absolute temperature, and F is the Faraday constant. The activity of ions a_{ion} is related to the activity coefficient γ_{ion} and the concentration C_{ion} as $a_{ion} = \gamma_{ion} C_{ion}$ for each kind of ions.

Some experimental efforts have been made to investigate the Donnan potential of polyelectrolyte hydrogels. An indirect method is measuring the osmotic pressure of polyelectrolyte hydrogels, from which the difference of solute ion concentration across the gel-solution boundary is estimated and the electrical potential is calculated.¹² Another method is to measure the electric conductance of polyelectrolyte hydrogels, and then estimate the fraction of counter-ions according to the equivalent conductance of the counter-ion in pure solvent solution.³ Fluorescent indicators were also used to detect proton concentration and therefore the electrical potential of acidic polyelectrolyte hydrogels.¹³ However, these methods are indirect and only give the average charge density of hydrogels. On the other hand, the zeta potential measurements give only averaged information of charged surfaces, but not any direct information of the bulk hydrogels.¹⁴

To map the spatial distribution of electric potential, electrode probes are a promising

technique. Electrode probes have been widely used to study the physical chemistry properties of polymer solution, such as pH¹⁵, impedance¹⁶, potentiometric titration¹⁷ etc. With microelectrode, the electrodes have also been adopted to study the electric signals in and out of neuron and muscle cells.¹⁸⁻²³ Naturally, Some studies have been performed to use the microelectrode technique (MET) to measure the 3D electric potential of polyelectrolyte hydrogels ^{5,24-30}.

Different from the case of solution or semi-liquid cells³¹, when applying the MET to measure the potential of hydrogels, the major difficulty is to make a good contact of the microelectrode to the hydrogels. Giving the solid-like nature of the hydrogels that has a network mesh size in nano-scale, inserting of the microelectrode causes fracture of the materials, which might give a poor local contact of the electrode to the hydrogel, and therefore, lead to underestimation of the potential. Especially, in the case of a brittle polyelectrolyte hydrogel, sharp crack might be formed at the tip of the capillary electrode. Because of this reason, previous studies on hydrogel using microelectrode technique failure to obtain the potential quantitatively, especially in the case of brittle polyelectrolyte gels.^{5, 26-29}

To apply MET for the accurate measurement of the electric potential distribution, a systematic study on the correlations between the potentials measured and the microelectrode geometry, the inserting speed, are needed, which is hardly done yet due to technical difficulties.³²

The objective of this study is to establish a microelectrode technique to quantitatively study the electrical potential of polyelectrolyte hydrogels. This paper is organized as

follows. First, we discuss the potential drop in the crack upon inserting of microelectrode and its effect on the potential measured; Then, we experimentally investigate the effects of the inserting speed of the microelectrode and the geometry of the capillary, including the diameter and wall thickness, on the measured electric potential of polyelectrolyte hydrogels. As a model system of polyelectrolyte hydrogels, chemically crosslinked poly (2-acrylamido-2-methylpropanesulfonic acid) (PAMPS) hydrogel is used. After that, we compare the experiment observation with the theoretical Donnan potential values taking consideration of the counter-ion condensation effect³³. Finally, we demonstrate the ability of the microelectrode method for the measurement of spatial distribution of electric potential by measuring the potential modulation of a multi-layer gel consisting of alternative stacking of oppositely charged polyelectrolyte gel layers. This MET method will provide a powerful tool to characterize the internal structure of polyelectrolyte gels in the swollen state directly without any structure labeling.

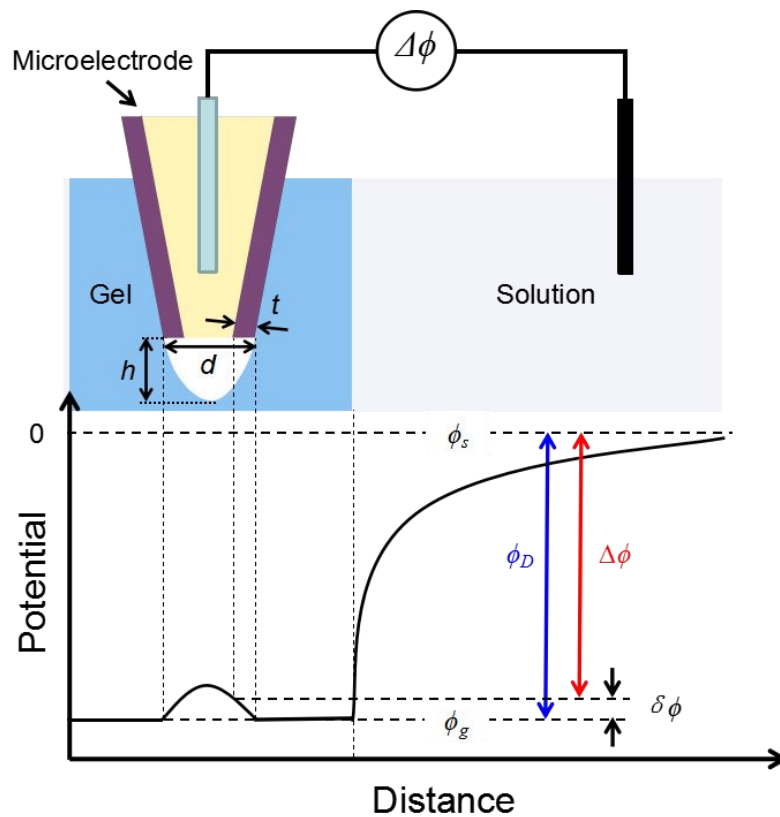
General consideration

Here we consider a negatively charged, brittle hydrogel immersed in salt solution as shown in **Scheme 2**. When a microelectrode of an out- diameter d is penetrated into the gel, the fracture of the gel induces a crack at the tip of the capillary with a crack length h . Comparing with the true Donnan potential ϕ_D , the potential measured ($\Delta\phi$) is small by a potential drop $\delta\phi$,

$$\Delta\phi = \phi_D - \delta\phi \quad (2)$$

The potential drop $\delta\phi$ is determined by the minimum distance r of the conductive solution phase (KCl solution) of the electrode to the fractured gel surface. This contact distance depends on the geometry of the capillary and the crack. When the wall thickness of the capillary t is shorter than the crack length h , $r = t$, as shown in **Scheme 2**. When h is shorter than t , $r = h$.

Since the distribution of counter-ions on the fractured surface of the hydrogel is confined within a distance of the Debye length, r_D , the potential drop also depends on the local Debye length around the capillary. Any improvements to decrease r or increase r_D will reduce the potential drop and increase the accuracy of the potential measurements.



Scheme 2. Schematic illustrations of the geometry and the potential distribution around the

tip of a microelectrode inserting in a brittle polyelectrolyte hydrogel carrying negative macro-ions. Inserting of the microelectrode generates a micro-crack and a potential perturbation. The potential measured by the microelectrode $\Delta\phi$ is reduced by a drop $\delta\phi$ in comparison with the Donnan potential ϕ_D . $\delta\phi$ is determined by the minimum distance r of the conductive solution phase (KCl solution) of the electrode to the fractured gel surface, i. e., $r = (t, h)_{\min}$. In this illustration, the case $t \ll h$ is shown.

Thus, it is intuitive to consider that the condition for accurate potential measurement is that

$$r = (t, h)_{\min} \ll r_D \quad (3)$$

Here r_D is the Debye length in the crack.

Assuming linear elastic fracture mechanics, the crack length of a *brittle gel* h is related with the modulus E , the Poisson's ratio ν , and the fracture energy Γ of the gel as (supporting information **Scheme S1**)

$$h = \frac{Ed^2}{8(1+\nu)\Gamma} \quad (4)$$

Therefore, h scales with the diameter d of the microelectrodes as $h \sim d^2$, and reducing of the capillary diameter d leads to a small crack length. Furthermore, the impact of volume exclusion by the inserting of the microelectrode, which perturbs the potential distribution, will also decrease with the decrease of the capillary diameter. On the other hand, as will be shown later experimentally, the capillary wall thickness t decreases linearly with the decrease of the capillary diameter d . Therefore, decreasing of the capillary diameter will increase the accurate of potential measurement.

Next, discuss the Debye length r_D in the cracked region. We will show that r_D is much larger than that of the bath solution r_D^s (Table 1). Considering a negatively charged polyelectrolyte gel with macro-ion concentration C_-^p , at the Donnan equilibrium, the electric chemical potentials of mobile ions in the gel and in the bath solution are the same. From this condition, the relationship between the concentration of salt in bath solution C_s , and that of the counter-ions C_+ and the co-ions C_- in gel is given by ¹¹:

$$C_s^2 = C_+ C_- \quad (5)$$

The electrically neutral condition of the gel gives

$$C_-^p + C_- = C_+ \quad (6)$$

When $C_-^p \gg C_s$, **Eqs. (5) and (6)** give $C_+ \approx C_-^p \gg C_s$ and $C_- \approx C_s^2 / C_-^p \ll C_s$.

This means that for a highly charged gel equilibrated in a bath solution of low ionic strength ($C_-^p \gg C_s$), the concentration of the counter-ion is much higher than that of the surrounding salt solution ($C_+ \gg C_s$), while the concentration of the co-ions is much lower than the salt concentration of the bath solution ($C_- \ll C_s$). When a crack is generated by inserting of the microelectrode, within a relatively short time, a new equilibrium should be reached locally in the cracked region. Just like the working mechanism of reverse osmosis³⁴, the very low co-ion concentration in the gel prevents the co-ions from effectively diffusing to the cracked region, and thus the cracked region has a very low ionic concentration due to electroneutrality. Consequently, the Debye length in the cracked region is much larger than that in the bath solution. This feature should favor the accurate measurement of the gel potential. For example, for a

gel with a macro-ion concentration $C_-^p = 10^{-1}$ M, if the concentration of KCl in bath solution is $C_s = 10^{-5}$ M, then the concentration of co-ions Cl^- in the gel is $C_- = 10^{-9}$ M, which is 4 orders lower in magnitude than the salt concentration in the bath solution. As the co-ion concentration is negligible, the Debye length of the cracked gel surface is determined by ion concentration of water. For common water, it has a $\text{pH} = 6.5$, which gives $r_D = 538.8$ nm, much larger than that of the bath solution ($r_D = 96$ nm, for KCl concentration $C_s = 10^{-5}$ M). Similarly, if KCl in bath solution is $C_s = 10^{-3}$ M, then Cl^- in the gel is $C_- = 10^{-5}$ M, the Debye length of the cracked gel surface is $r_D = 96$ nm, one order larger than that of the bath solution ($r_D = 9.6$ nm, for KCl concentration $C_s = 10^{-3}$ M).

Table 1. Ion concentrations and Debye lengths in bath solution and in the micro-crack taking consideration of the reverse osmosis effect. The data are for a polyelectrolyte gel carrying negative macro-ions of concentration $C_-^p = 0.1$ M. C_s , C_+ , C_- are concentrations of small ions in bath solution, counter-ions, co-ions of gel, respectively. r_D^s and r_D are the corresponding Debye length of bath solution and crack, respectively. When C_s is very low, the r_D in the crack is estimated from the pH of water.

C_s / M	r_D^s / nm	C_+ / M	C_- / M	r_D / nm
10^{-5}	96	10^{-1}	10^{-9}	538.8 (water, $\text{pH} = 6.5$)
10^{-3}	9.6	10^{-1}	10^{-5}	96

Experiment

Materials

2-Acrylamido-2-methylpropanesulfonic acid (AMPS) was a courtesy from Toa Gosei Co., Ltd. Acryloyloxethyltrimethylammonium chloride (DMAEA-Q), 78.8 wt%, was a courtesy from MT AquaPolymer, Inc., N,N'-methylenebisacrylamide (MBAA), 2-oxoglutaric acid (OA), and potassium chloride (KCl) were purchased from Wako Pure Chemical Industries, Ltd. All these materials were used as received.

Synthesis of PAMPS hydrogels

PAMPS hydrogels with different cross-linking densities were prepared by radical polymerization initiated by UV irradiation. A precursor aqueous solution containing monomer (AMPS: 1 M), cross-linker (MBAA: 0.5, 1, 2, 3, 4 and 5 mol% in relative to AMPS concentration), and initiator (OA: 0.1 mol% in relative to AMPS concentration), was poured into a reaction cell consisting of two glasses spaced with 2 mm silicone rubber. PAMPS hydrogels were obtained after photo-polymerization for 8 h under argon atmosphere. The conversion ratio of AMPS was studied by measuring the conductivity of washing solution, and comparing it to the standard AMPS conductivity curve by conductivity meter (FE30 KIT, Mettler-Toledo). The as-prepared PAMPS hydrogels were immersed in deionized water and the immersion water was changed every day for more than one week to for the complete removal of the residual monomers or initiators. After that, the swollen PAMPS hydrogels of 3 ~ 5 mm thickness were immersed in KCl solutions of prescribed concentration for at least 2 days to reach equilibrium. The PAMPS gels were coded as PAMPS- C_{MBAA} , where

C_{MBAA} was the crosslinking density in mol% in relative to the AMPS monomer concentration in preparation.

The swelling ratio was calculated by the volume change as $Q = V/V_0$, where V and V_0 are the volumes of the swollen gel and the as-prepared gel, respectively. The dimensions of each sample were measured for three times. The equilibrium swelling ratios of the PAMPS hydrogels synthesized with different cross-linking densities were shown in supporting information **Fig. S1**. Since the conversion ratio of polymerization was higher than 98%, the concentration of the AMPS in the swollen gel C_{AMPS} was calculated from the AMPS concentration of the precursor solution $C_{AMPS,0}$ (=1 M) by the relationship $C_{AMPS} = C_{AMPS,0} / Q$. The swelling ratio Q of PAMPS gels in pure water and the concentration of AMPS in the swollen gel C_{AMPS} are shown in Table 2.

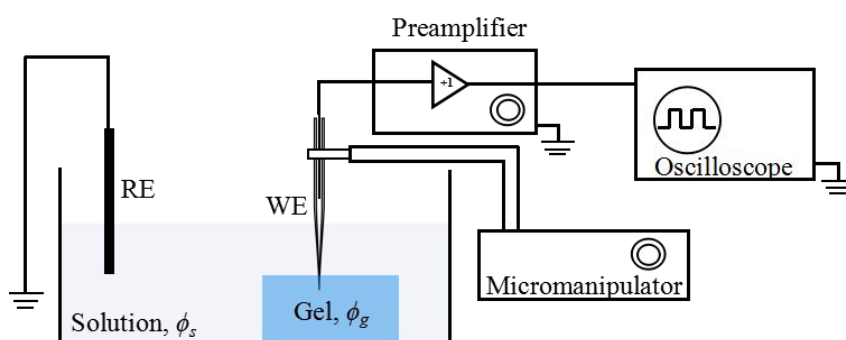
Table 2. Swelling volume ratio, Q , AMPS concentration, C_{AMPS} , for fully water-swollen PAMPS gels prepared at various cross-linker density, C_{MBAA} .

C_{MBAA} (mol%)	0.50	1.00	2.00	3.00	4.00	5.00
Q (V/V)	522.6	147.6	43.7	22.9	14.5	10.8
C_{AMPS} (M)	0.0019	0.0068	0.023	0.044	0.069	0.093

The multi-layer gel consisting of alternative stacking of negatively and positively charged gel layers was prepared from ultra-thin negative PAMPS gel and positive PDMAEA-Q gel. These thin film gels were synthesized with 0.1 mm silicone spacer

in glass cell. Typically, UV initiated polymerization was carried out with a precursor solution containing monomer (2 M), cross-linker (MBAA: 4 mol% in relative to monomer), and initiator (OA: 0.1 mol% in relative to monomer) for 8 h under argon atmosphere.

Potential measurement setup



Scheme 3. Experimental setup for potential measurement. The setup is composed of three parts: (1) electrodes: a working microelectrode (WE) and a reference electrode (RE) are used for potential measurement; (2) micromanipulator: the WE is controlled to insert into gel with a constant velocity; (3) recording system: the electrical signals are amplified by preamplifier and recorded by an oscilloscope.

The experimental setup for electrical potential measurement of gels is shown in **Scheme 3**. The system has two electrodes, a reference electrode (RE) and a working electrode (WE). Both RE and WE are home-made glass microelectrodes. The RE was inserted in the KCl bath solution and electrostatically grounded. The WE was inserted into the hydrogel immersed in the KCl bath solution at a constant speed controlled by a micromanipulator (DMA-1511, Narishige). The WE was connected to an oscilloscope (Iwatsu, DS-4264) via a high-impedance intracellular preamplifier

(Model 8700 Cell Explorer, Dagan) to measure the electric potential. The gels of 3 ~ 5 mm thickness were equilibrated in the KCl bath solution for 2 days before measurement. The inserting speed of the electrode can be precisely controlled in the range of 395-7900 nm/s by the micromanipulator. The spatial resolution in depth profile of inserting direction was 5 nm, which was determined by the accuracy of the micromanipulator. The system was placed on an anti-vibration table in a room with anti-electric noise protection. The following special cautions were paid in the measurement. (1) the Ag/AgCl wires were immobilized to glass capillary for both WE and RE; (2) the setup was covered with a shield (dimension of 40×45×50 cm³) to reduce the influence of electromagnetic interference during potential measurement; (3) the gel was fixed to the container of the bath solution by micro-metal needles; (4) the residual monomers in the gel was thoroughly removed by prolonged dialysis. It took more than 1 week for the complete removal of residual chemicals, which was confirmed by detecting the conductivity change of bath solution using a conductivity meter (FE30 KIT, Mettler-Toledo).

Preparation of working electrode

The working electrodes were prepared by inserting a reversible silver/silver chloride electrode (Ag/AgCl) into a glass micropipette with a tip diameter < 1 μm. Then, the glass micropipettes were filled with 3 M KCl solution. The thin glass micropipettes were prepared by pulling a borosilicate capillary tube (outer diameter 1.0 mm, inner diameter 0.78 mm, Sutter Instrument Co.) using a horizontal automatic micropipette

puller (P-2000, Sutter Instrument Co.). The diameter of micropipettes was controlled by adjusting various parameters of puller. The diameter of the micropipettes can be controlled with an accuracy of ~ 20 nm in standard deviation.

In order to characterize the diameter and wall thickness of microelectrode precisely, transmission electron microscope (TEM) (H-7650, Hitachi) was used to observe the morphology of the microelectrodes mounted on a home-made holder (see supporting information **Fig. S2**). The TEM images were taken with an accelerating voltage of 100 kV.

A 7-barrel electrode was also prepared by pulling 7-barrel capillary (outer diameter 3.0 mm, inner diameter 0.58 mm for each channel, World Precision Instruments, Inc.) with vertical puller (PE-21, Narishige). Each barrel capillary was filled with 3 M KCl solution before inserting of Ag/AgCl wires. The dimension of 7-barrel electrode was observed by scanning electron microscope (SEM, JEOL Ltd., JSM-6010LA), and the outer diameter of 7-barrel electrode was found to be about 550 nm (supporting information **Fig. S3**).

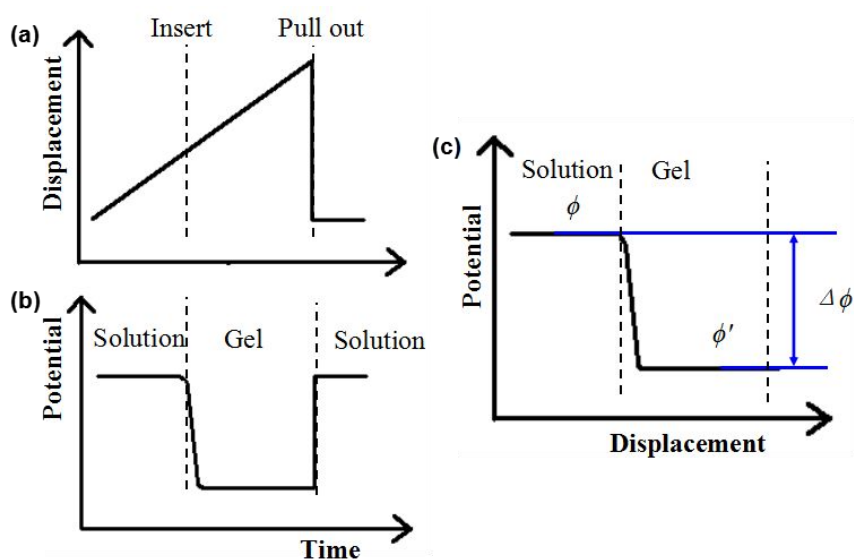
Potential measurement of PAMPS hydrogels

Unless specifically mentioned, the electric potential was measured by using the single electrode as WE. All the measurements were performed at 25 °C. For 3 M KCl filled microelectrodes in 10^{-5} M KCl solution, the junction potential was usually within 5 mV.²²

For the 7-barrel electrode, each single microelectrode serves as a WE, and potential of

hydrogels was detected separately by 7-barrel electrode in each channel.

Scheme 4 shows the illustration to obtain the depth profile of the electric potential of the gel. With inserting of the microelectrode (WE) to the negatively charged PAMPS gel at a steady speed (**Scheme 4 (a)**), the potential difference between the WE and RE abruptly drops from zero to a stable negative value with the time (**Scheme 4 (b)**). Conversely, when the microelectrode is withdrawn from the hydrogel at a much quick speed, the negative potential vanishes to zero value instantly (**Scheme 4 (b)**).



Scheme 4. Procedures to obtain the potential - displacement curve. (a) The microelectrode is inserted into hydrogels at a constant velocity and a tip displacement-time relation is obtained; (b) the electrical signals are recorded over time. When the microelectrode is inserted into the gel, a potential change is observed, and when the microelectrode is pulled out from the hydrogel, the potential recovers to its reference value; (c) The potential - displacement curve is obtained by combining data of (a) and (b).

For a constant inserting velocity of WE, the depth profile of the potential of hydrogel

from surface to bulk is obtained from the time profiles by converting the time to displacement of WE (**Scheme 4 (c)**). The electric potential difference between the gel at the measuring position ϕ' and the bath solution ϕ , is denoted as $\Delta\phi = \phi' - \phi$. In this work, we adopted the average potential $\Delta\phi$ from the depth profile of the sample within 200 μm to the sample surface, and the error bar was the standard deviation of the average. It was confirmed that when the same microelectrode (diameter ~ 190 nm) was used, the potential variation of the same hydrogel at different positions (PAMPS-4 hydrogel in 10^{-5} M KCl solution) had a standard deviation of 6 mV.

Results and discussion

1. Potential profile

Fig. 1 shows a typical potential depth profile of PAMPS-4 hydrogel measured by a microelectrode with a diameter of 180-200 nm at an insertion speed of 395 nm/s. In the solution, the potential was nearly constant. At the gel-solution interface, when the microelectrode tip was crossing the interface from the solution side, the measured potential showed a gradual decrease followed by an abrupt one. Deep inside the bulk of gel, the potential exhibited a nearly constant value again. Slight fluctuation of the potential was observed in the bulk gel, which may be related to both the heterogeneity in the structure of PAMPS networks or the possible fracture instability of PAMPS networks. The average potential value of the bulk PAMPS hydrogel was found to be $\Delta\phi = -184 \pm 3$ mV.

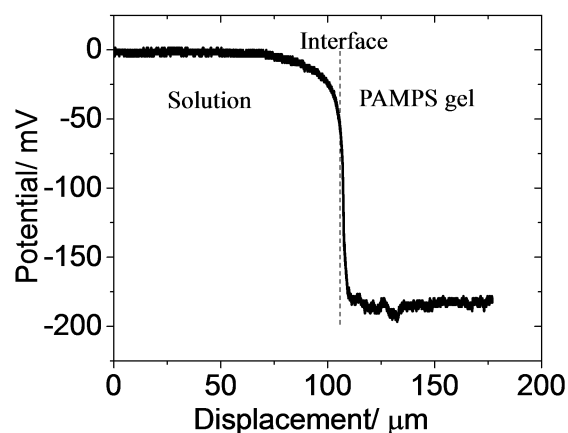


Figure 1. A typical potential - displacement curve. Sample: PAMPS-4 gel, bath solution: 10^{-5} M KCl, microelectrode diameter $d=190$ nm, wall thickness $t=21$ nm.

In order to verify if the leakage of KCl solution from the microelectrode occurred and reduced the measured potential value, we also observed the time profile of the potential at a fixed penetration depth of $100 \mu\text{m}$. We found that within 80 s, there is no change or decay in the potential, indicating that leakage effect could be neglected during measurement (supporting information **Fig. S4**).

2. Effect of microelectrode insertion velocity

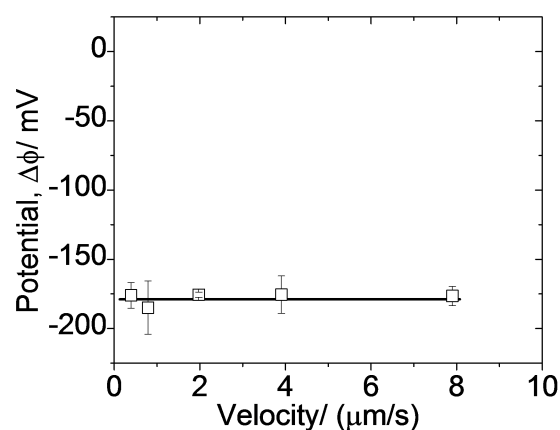


Figure 2. Potential measured at various inserting velocities. Sample: PAMPS-4 gel, bath

solution: 10^{-5} M KCl, microelectrode diameter $d=190$ nm, wall thickness $t=21$ nm. Potential was found to be velocity-independent.

Fig. 2 shows the potential of the PAMSP-4 gel measured at various insertion velocity using electrodes of diameter about 190 nm. The average potential was found to be approximately -180 mV, independent of the insertion velocity. This result did not contradict with the viscoelasticity or poroelasticity of the gel³⁵. With permanent chemical crosslinks, the PAMPS hydrogels are mostly elastic within the time scale of interest, so that their fracture behavior is rate independent. On the other hand, the poroelastic relaxation time is related to both mesh size and the collective diffusion coefficient of the polymer networks. For example, taking the representative value of the collective diffusion constant D of the gel is $D=10^{-9}$ m²/s,³⁶ the characteristic swelling time³⁷ of a 100 μ m thin gel is ~ 10 s . The insertion process is slow enough that a local equilibrium is attained (it will take ~ 253 s to reach a 100 μ m depth for microelectrode). Therefore, the observed potential is independent of the inserting speed. In the following experiment, the inserting velocity was fixed at 395 nm/s unless otherwise specified.

3. Effect of microelectrode diameter

Previous discussion has shown that the accuracy of the electric potential measured is related to the shortest distance of the electric probe to the fractured gel surface r , which is determined by $r = (t, h)_{\min}$. The crack length h scales with the

microelectrode diameter d as $h \sim d^2$. The microelectrode wall thickness t should also strongly depend on the diameter of the microelectrode d . We prepared single-barrel microelectrodes of diameters in the range 190 nm \sim 4750 nm (supporting information **Fig. S5 (a)**). The microelectrode wall thickness t was found to be linearly proportional to the diameter d (supporting information **Fig. S5 (b)**),

$$t = 0.11d \quad (7).$$

This correlation is due to the equal pulling deformation of the electrode during preparation. Although we could not directly measure the value of h , the d dependence of measured potential will tell us which parameter, h or t , determines the shortest distance between the electrode probe and the gel surface r .

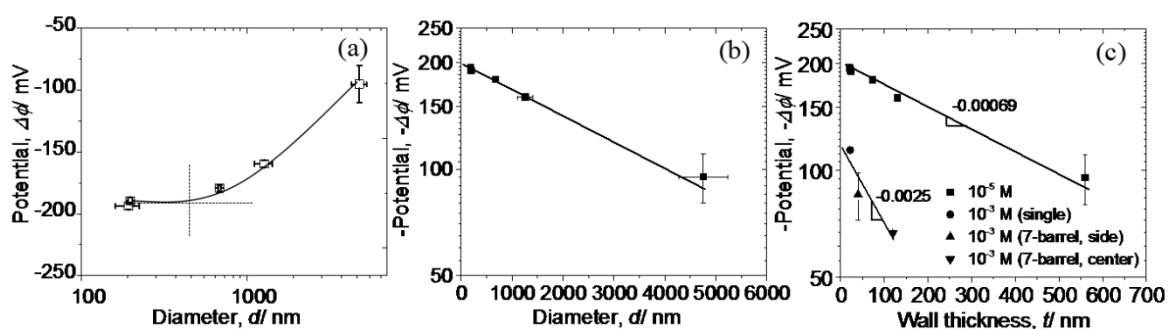


Figure 3. Potential of PAMPS-4 hydrogel measured using microelectrodes of different diameters. (a) The potential showed dependence on the outer diameter d of the microelectrode. When $d < 400$ nm, the potential $\Delta\phi$ becomes almost constant, independent of d ; (b) Semi-log plot of $\Delta\phi$ and d . A linear correlation between $\log(-\Delta\phi)$ and d is observed, which suggests that the potential is related to the wall thickness t that is linearly related to d as $t=0.11d$; (c) Semi-log plot of $\Delta\phi$ and the wall thickness t . The data points marked by “ \blacktriangle ” and “ \blacktriangledown ” were measured by the side and central electrodes of the 7-barrel electrode, respectively. In both 10^{-3} M

and 10^{-5} M KCl solution, the potential shows linearity to t in the semi-log plot; The potential decreases more rapidly with increase of t in high KCl solution. Characteristic decay lengths l_D obtained from the slope of the straight lines are 633 nm and 175 nm, for 10^{-5} M and 10^{-3} M KCl bath solution, respectively. These decay lengths are close to the Debye lengths r_D around the microelectrode taking consideration of the reverse osmosis effect (Table 1).

Fig. 3 (a) shows the potential of a PAMPS-4 gel equilibrated in a 10^{-5} M KCl solution, measured with electrodes of various diameters at an inserting speed of 395 nm/s. The absolute potential value $\Delta\phi$ increases when the diameter d decreases, and approaches to a constant value at $d < 400$ nm. As shown in **Fig. 3 (b)**, the plot of $\log(-\Delta\phi) \sim d$ shows a linear correlation. This result suggests that the shortest distance of the electric probe to the fractured gel surface r is related to the microelectrode wall thickness t , not the crack length h , since t is related to d linearly while h scales with d as $h \sim d^2$. That is, $r = (t, h)_{\min} = t$. So we replot the potential data against t , which also shows a straight line, as shown in **Fig. 3 (c)**. That is, the measured potential and wall thickness is experimentally related by

$$\Delta\phi = \phi_0 \cdot \exp\left(-\frac{t}{l_D}\right) \quad (8)$$

Here, ϕ_0 is the extrapolated potential on the surface of the gel, l_D is a decay length. From the slope and the intercept of the line, we obtained $\phi_0 = -200$ mV and $l_D = 633$ nm from **Fig. 3 (c)**. The characteristic decay length thus obtained is much larger than the Debye length of the bath solution ($r_D^s = 96$ nm, for KCl concentration $C_s = 10^{-5}$ M), and comparable to that in the crack tip $r_D = 539$ nm considering the reverse osmosis

effect in the crack (Table 1).

4. Potential of PAMPS hydrogel measured by 7-barrel electrode

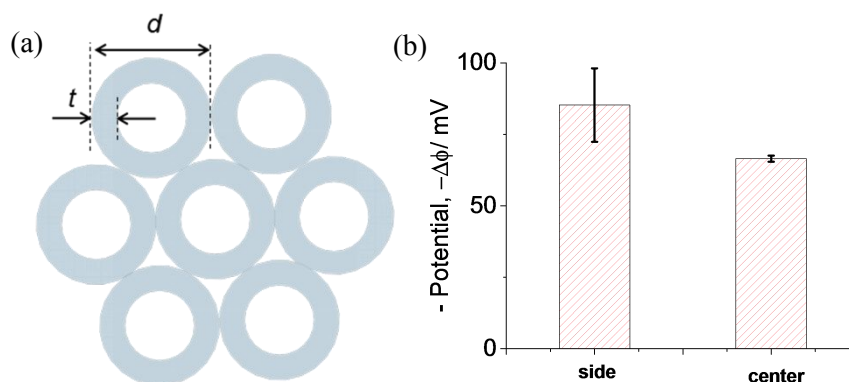


Figure 4. Potentials measured by 7-barrel electrode. (a) Illustration of cross-section of 7-barrel electrode, the wall thickness t of each barrel electrode is ~ 40 nm, the diameter of each electrode d is ~ 180 nm; (b) Potential of a PAMPS-4 hydrogel measured by 7-barrel electrode in 10^{-3} M KCl solution, the average values of 6 side electrodes and center electrode are shown. The effective wall thickness of the central electrode is $40 \text{ nm} \times 3 = 120 \text{ nm}$.

To further confirm that the wall thickness t determines the measured potential, we adopt a 7-barrel electrode to measure the potential of a PAMPS-4 gel equilibrated in 10^{-3} M KCl solution. As shown in **Fig. 4 (a)**, the 7-barrel electrode contains one central electrode with six hexagonally arranged side electrodes. The outer diameter and wall thickness of each electrode is $d \sim 180$ nm and $t \sim 40$ nm, respectively. Although the shortest distance of the central electrode wall to the fractured surface is 220 nm, the effective wall thickness or distance is $40 \text{ nm} \times 3 = 120 \text{ nm}$, considering the electric conductive property of the KCl solution in the side electrodes. The

potential measurement was carried out at each channel separately, and the averaged potential value over 6 side electrodes and the potential of the central electrode were shown in **Fig. 4 (b)**. The absolute potential of the central electrode is found to be lower than that of the side electrodes.

We also plot the potential data of the PAMPS-4 gel measured by 7-barrel electrode equilibrated in 10^{-3} M KCl against the effective wall to the fractured gel surface, in **Fig. 3 (c)**. An exponential correlation between the potential and the effective wall thickness is also observed, confirming that the wall thickness t determines the potential result. **Fig. 3 (c)** also shows that in a high salt concentration, the absolute potential becomes low and the wall thickness dependence of the potential becomes strong, corresponding to a short decay length l_D . From the slope and the intercept at zero wall thickness, we obtained $l_D \sim 175$ nm and potential $\phi_0 = -120$ mV. This l_D is also much longer than the Debye length of the bath solution ($r_D^s = 9.6$ nm for $C_s = 10^{-3}$ M) and about two times of the Debye length $r_D = 96$ nm in the crack (Table 1).

As a summary, the potential measured is related to the wall thickness of the capillary. This is considered as a feature of the brittle gel that forms a large crack length. For ductile gels, however, the fracture geometry at the crack tip is very different and should be studied separately in future.

5. Quantitative comparison of the observation with the theory

What is the physical meaning of the potential ϕ_0 thus measured? The most

reasonable answer is that ϕ_0 is the Donnan potential. To justify this answer, we measured the potential of gels with different charge concentration $C_-^p = C_{AMPS}$ (M) in 10^{-5} M KCl solution, and made a quantitative comparison of the observed potential with the Donnan potential obtained theoretically. The charge concentration was tuned by varying the chemical cross-linker density of the gel (Table 2). For simplicity, we adopt microelectrode of small diameter ($d \sim 190$ nm) for the measurement and the potential thus measured is adopted as ϕ_0 . This is because **Fig. 3 (a)** tells that the potential measured by the microelectrode of diameter less than $d=400$ nm is approximately equal to ϕ_0 . As shown in **Fig. 5**, the potential of the PAMPS hydrogels linearly decreases with increase of charge concentration, C_{AMPS} , in a semi-log plot.

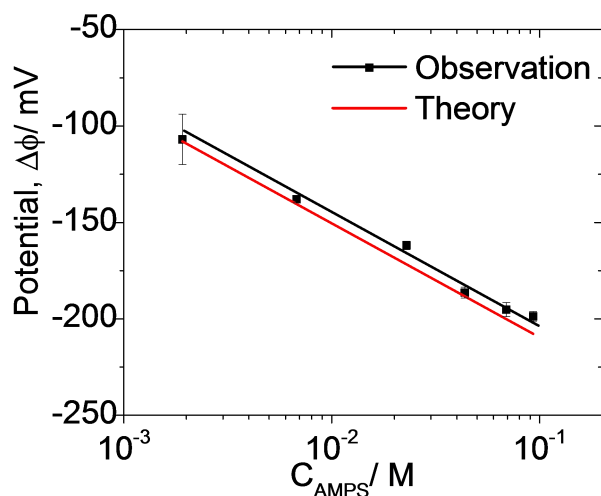


Figure 5. Electric potential of PAMPS hydrogels with various charge concentrations. The theoretical curve is calculated according to Donnan equation taking consideration of the counter-ion condensation effect. Activity coefficient γ_{ion} of 0.35 and 1.0 were used for the counter-ions of the gel and of the bath solution, respectively. Bath solution: $C_s=10^{-5}$ M KCl, microelectrode diameter $d=190$ nm, wall thickness $t=21$ nm.

The theoretical potential value of the PAMPS hydrogels at the Donnan equilibrium can be estimated from the concentration ratio of small ions inside and outside of the gel taking consideration of their activity coefficients, using **Eq. (1)**. As the concentration of the co-ion Cl^- inside the PAMPS hydrogels equilibrated in 10^{-5} M KCl solution is negligible, the counter-ion K^+ concentration is equal to the fixed macro-ion concentration C_{AMPS} that is shown in Table 2. The main factor to influence the activity coefficient of counter-ions in the highly charged polyelectrolyte gels is the counter-ion condensation effect³⁸. For the PAMPS system, the two adjacent charges of AMPS monomer extend over roughly 0.25 nm (l_0) and Bjerrum length (l_B) in pure water is 0.712 nm,³³ therefore the effective counter-ions is about $l_0/l_B = 0.35$ of all counter-ions. If we assume that the activity coefficient only comes from the counter-ion condensation effect, the activity coefficient of counter-ions can be roughly considered as $\gamma_{K^+}^g = 0.35$. On the other hand, the activity coefficient of K^+ in bath solution is $\gamma_{K^+}^s = 1$, considering the diluted concentration ($C_{K^+} = 10^{-5}$ M). The Donnan potential theoretically calculated using these activity coefficients is also shown in **Fig. 5**. We found that the observed potential values are very close to the theoretical prediction, indicating that the potential ϕ_0 measured corresponds to the Donnan potential. Thus, using a microelectrode of less than 200 nm in diameter, Donnan potential of polyelectrolyte gels are able to be measured accurately.

6. Potential profile of multi-layers of negative/positive hydrogels

Since this microelectrode technique gives depth profile of electric potential, it is able

to accurately study the spatial distribution of potential. To demonstrate this, we constructed a multi-layer gel consisting of alternative stacking of two oppositely charged hydrogels, negatively charged PAMPS and positively charged PDMAEA-Q (Fig. 6 (a)). These unit layers are adhered spontaneously together by electrostatic interaction. The depth profile of potential of this sample equilibrated in 10^{-5} M KCl solution is shown in Fig. 6 (b). The PAMPS gel layers and the PDMAEA-Q gel layers show potential of $-189 \sim -191$ mV and $150 \sim 166$ mV, respectively. From the potential profile, the thickness of each layer can be accurately determined by this measurement, about $163 \sim 165$ μm and $163 \sim 173$ μm for PAMPS and PDMAEA-Q gels, respectively.

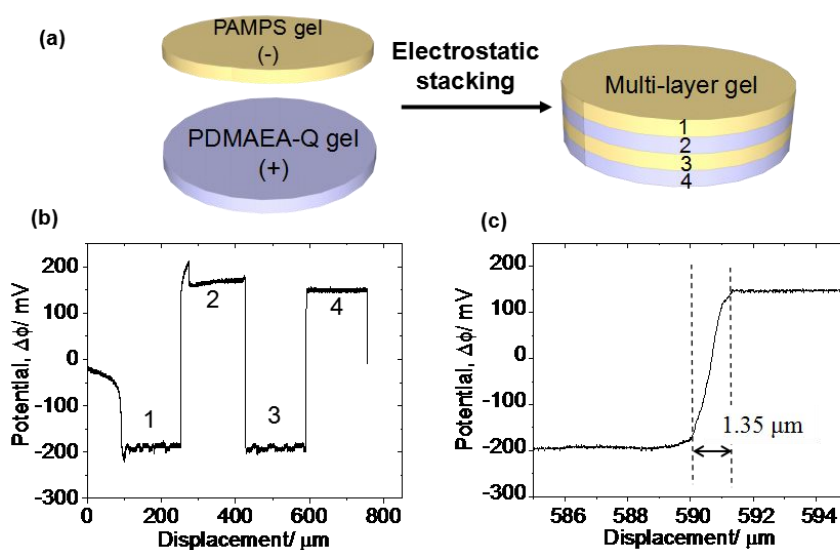


Figure 6. Measurement of the electric potential distribution in a multi-layer gel. (a)

Schematics of assembly of oppositely charged hydrogels by electrostatic interaction; (b) Depth

profile of electric potential of the multi-layer gel, 1 and 3 represent PAMPS layers; 2 and 4

represent PDMAEA-Q layers; (c) Magnified potential profile at the transition region from

negative to positive layers (layer 3 to layer 4). Bath solution: 10^{-5} M KCl, microelectrode diameter

$d=190$ nm, wall thickness $t=21$ nm.

At the boundary, the two oppositely charged layers form polyion complex to give a neutral layer of mesh size thickness. This is equivalent to the case that a neutral nano-gel layer is sandwiched by two oppositely charged gel layers. The transition length at the boundary between oppositely charged layers can be determined precisely from the depth profile of potential. As a typical example, **Fig. 6 (c)** shows an enlarged depth profile between layer 3 and layer 4. The transition length δ was found much larger than the mesh size of the gel network, and almost the same for inserting from negative to positive layers ($\delta_{1/2}=1.08 \mu\text{m}$, $\delta_{3/4}=1.35 \mu\text{m}$) and from the positive to negative layers ($\delta_{2/3}=1.58 \mu\text{m}$). This result suggests that transition length observed is truly a structural property of the gel, not related to measurement. As both the PAMPS layer and the PDMAEA-Q layer have a Debye length of about $r_D=633 \text{ nm}$ (Table 1), it is reasonable to consider that the transition length is the summation of the Debye length of the two layers, that is $\delta=2r_D$. The result demonstrates the excellent ability of the microelectrode technique to measure the spatial distribution of electric potential.

Conclusions

The potential of a brittle polyelectrolyte hydrogel is measured by the microelectrode technique (MET). The potential thus measured is independent of the inserting velocity of the microelectrode but it exponentially decays with the capillary wall thickness of the microelectrode. The characteristic decay length is comparable to the Debye length

of the crack region, much larger than the Debye length of the bath solution. Using a thin capillary of diameter ~ 200 nm and wall thickness ~ 20 nm, the measured potential is well in agreement with the Donnan potential theoretically predicted for the polyelectrolyte gel in dilute salt solution. This result demonstrates that the microelectrode technique can quantitatively measure the spatial distribution of Donnan potential of polyelectrolyte hydrogels. The results also show that the true Donnan potential can be obtained by extrapolating the data measured by several relatively thick microelectrodes using an exponential function. Unlike traditional osmotic pressure method that can only give average potential values of hydrogel, MET can accurately detect the depth profile of potential of hydrogels from surface to bulk. It provides a powerful tool to characterize the heterogeneous hydrogel systems, such as interface of polyelectrolyte multi-layers, gradient membranes, and internal fracture-induced structure changes of double network (DN) hydrogels, which will be reported by separate works.

Acknowledgments

This research was financially supported by a Grant-in-Aid for Scientific Research (S) (No. 124225006) from the Japan Society for the Promotion of Science (JSPS). H. L. G. thanks the MEXT for the scholarship. The authors would like to thank Dr. Yumihiko Ikura, Dr. Taolin Sun, Dr. Daniel R. King, Mr. Riku Takahashi, Mr. Ping Rao, Mr. Taiki Fukuda and Mr. Xiaotian Si for their kind discussion and help.

Reference

1. Osada, Y.; Gong, J. P., Soft and wet materials: Polymer gels. *Adv Mater* **1998**, *10* (11), 827-837.
2. Liu, X. X.; Tong, Z.; Hu, O., Swelling Equilibria of Hydrogels with Sulfonate Groups in Water and in Aqueous Salt-Solutions. *Macromolecules* **1995**, *28* (11), 3813-3817.
3. Gong, J. P.; Komatsu, N.; Nitta, T.; Osada, Y., Electrical conductance of polyelectrolyte gels. *J Phys Chem B* **1997**, *101* (5), 740-745.
4. English, A. E.; Tanaka, T.; Edelman, E. R., Equilibrium and non-equilibrium phase transitions in copolymer polyelectrolyte hydrogels. *J Chem Phys* **1997**, *107* (5), 1645-1654.
5. T.F. Shklyar, A. P. S., O.A. Toropova, G.H. Pollack, and F.A. Blyakhman, Mechanoelectric potential in synthetic hydrogels: possible relation to Cytoskeleton. *Cell Biophysics* **2010**, *66* (6), 1014-1021.
6. Gong, J. P.; Kagata, G.; Osada, Y., Friction of gels. 4. Friction on charged gels. *J Phys Chem B* **1999**, *103* (29), 6007-6014.
7. Gong, J. P.; Iwasaki, Y.; Osada, Y.; Kurihara, K.; Hamai, Y., Friction of gels. 3. Friction on solid surfaces. *J Phys Chem B* **1999**, *103* (29), 6001-6006.
8. Gong, J. P.; Katsuyama, Y.; Kurokawa, T.; Osada, Y., Double-network hydrogels with extremely high mechanical strength. *Adv Mater* **2003**, *15* (14), 1155-+.
9. Tiyaipiboonchaiya, C.; Pringle, J. M.; Sun, J. Z.; Byrne, N.; Howlett, P. C.; Macfarlane, D. R.; Forsyth, M., The zwitterion effect in high-conductivity polyelectrolyte materials. *Nat Mater* **2004**, *3* (1), 29-32.
10. Kikuchi, A.; Okano, T., Pulsatile drug release control using hydrogels. *Adv Drug Deliver Rev* **2002**, *54* (1), 53-77.

11. David Eisenberg, D. C., *Physical Chemical with applications to the life science*, The Benjamin/Cummings Publishing Company, INC.: California, 1979; p 389.
12. Horkay, F.; Tasaki, I.; Basser, P. J., Osmotic swelling of polyacrylate hydrogels in physiological salt solutions. *Biomacromolecules* **2000**, *1* (1), 84-90.
13. Sawahata, K.; Gong, J. P.; Osada, Y., Soft and Wet Touch-Sensing System Made of Hydrogel. *Macromol Rapid Comm* **1995**, *16* (10), 713-716.
14. Yezek, L. P.; van Leeuwen, H. P., An electrokinetic characterization of low charge density cross-linked polyacrylamide gels. *J Colloid Interf Sci* **2004**, *278* (1), 243-250.
15. Sigel, H.; Zuberbuhler, A. D.; Yamauchi, O., Comments on Potentiometric Ph Titrations and the Relationship between Ph-Meter Reading and Hydrogen-Ion Concentration. *Anal Chim Acta* **1991**, *255* (1), 63-72.
16. Bobacka, J.; Lewenstam, A.; Ivaska, A., Electrochemical impedance spectroscopy of oxidized poly(3,4-ethylenedioxythiophene) film electrodes in aqueous solutions. *J Electroanal Chem* **2000**, *489* (1-2), 17-27.
17. Morcelletsauvage, J.; Morcellet, M.; Loucheux, C., Polymethacrylic Acid-Derivatives .3. Potentiometric and Conductimetric Titrations of Poly-[N-Methacryloyl-L-Alanine-Co-N-Phenylmethacrylamide] and Poly[Methacrylic Acid-Co-Benzyl Methacrylate]. *Makromol Chem* **1982**, *183* (4), 831-837.
18. Aonuma, H.; Nagao, T.; Nagayama, T.; Takahata, M., Modulatory effects of amino acids on neuromuscular transmission on the crayfish fast flexor muscle. *J Exp Zool* **1999**, *283* (6), 531-540.

19. Chang Won Lee, A. A. S., Yuji Ikegaya, and Zoran Nenadic, The Accuracy and Precision of Signal Source Localization with Tetrodes. *35th Annual International Conference of the IEEE EMBS, Osaka* **2013**.
20. Takahata, T.; Hayashi, M.; Ishikawa, T., SK4/IK1-like channels mediate TEA-insensitive, Ca²⁺-activated K⁺ currents in bovine parotid acinar cells. *Am J Physiol-Cell Ph* **2003**, *284* (1), C127-C144.
21. Aonuma, H.; Nagayama, T.; Takahata, M., Distribution of autofluorescent cell bodies in the crayfish central nervous system. *J Exp Zool* **1996**, *275* (6), 406-412.
22. Purves, R. D., *Microelectrode Methods for Intracellular Recording and Ionophoresis*. Academic Press: London, 1981; p 33.
23. Elliott, G. F.; Bartels, E. M., Donnan Potential Measurements in Extended Hexagonal Poly-Electrolyte Gels Such as Muscle. *Biophys J* **1982**, *38* (2), 195-199.
24. T.A. Davis, L.P. Yezek, J.P. Pinheiro and H.P. van Leeuwen, Measurement of Donnan potentials in gels by in-situ microelectrode voltammetry”, *J. Electroanal. Chem.* **2005**, *584*, 100-109.
25. K. Yasadi, J.P. Pinheiro, K. Zielinska, R.M. Town and H.P. van Leeuwen, Partitioning of humic acids between aqueous solution and hydrogel. 3. Microelectrode dynamic speciation analysis of free and bound metal complexes in the gel phase, *Langmuir* **2015**, *31*, 1737 -1745.
26. Gao, F.; Reitz, F. B.; Pollack, G. H., Potentials in anionic polyelectrolyte hydrogels. *J Appl Polym Sci* **2003**, *89* (5), 1319-1321.
27. Rainer W. Gülich, J. H. d., Andrea Weiblea, Thomas Wallmerspergerb, Bernd Kröplinb, Polyelectrolyte gels in electric fields A theoretical and experimental approach. *Smart Structures and Materials 2000: Electroactive Polymer Actuators and Devices (EAPAD)*, **2000**, *3987*, 193-202.

28. Safronov, A. P.; Kamalov, I. A.; Shklyar, T. F.; Dinislamova, O. A.; Blyakhman, F. A., Activity of counterions in hydrogels based on poly(acrylic acid) and poly(methacrylic acid): Potentiometric measurements. *Polym Sci Ser a+* **2012**, *54* (11), 909-919.
29. Shklyar, T. F.; Dinislamova, O. A.; Safronov, A. P.; Blyakhman, F. A., Effect of cytoskeletal elastic properties on the mechanoelectrical transduction in excitable cells. *J Biomech* **2012**, *45* (8), 1444-1449.
30. Katsiaryna Prudnikova and Marcel Utz, Electromechanical Equilibrium Properties of Poly(acrylic acid/ acrylamide) Hydrogels, *Macromolecules* **2012**, *45*, 1041–1045.
31. Wightman, R. M., Probing cellular chemistry in biological systems with microelectrodes. *Science* **2006**, *311* (5767), 1570-1574.
32. DiMaio, S. P.; Salcudean, S. E., Needle insertion modeling and simulation. *Ieee T Robot Autom* **2003**, *19* (5), 864-875.
33. Michel Daune, *Molecular Biophysics: Structures in motion*, Oxford University Press, 1999; p 331.
34. A.E. Yaroshchuk, Osmosis and reverse osmosis in fine-porous charged diaphragms and membranes, *Advances in Colloid and Interface Science* **1995**, *60*, 1-93.
35. Yue, Y. F.; Kurokawa, T.; Haque, M. A.; Nakajima, T.; Nonoyama, T.; Li, X. F.; Kajiwarra, I.; Gong, J. P., Mechano-actuated ultrafast full-colour switching in layered photonic hydrogels. *Nat Commun* **2014**, *5*.
36. Zi Liang Wu, Riku Takahashi, Daisuke Sawada, Md. Arifuzzaman, Tasuku Nakajima, Takayuki Kurokawa, Jian Hu, and Jian Ping Gong, In Situ Observation of Ca²⁺ Diffusion-Induced Superstructure Formation of a Rigid Polyanion, *Macromolecules* **2014**, *47*, 7208–7214.
37. Thomas E. Andreoli, Joseph F. Hoffman, Darrell D. Fanestil and Stanley G. Schultz, Membrane physiology, *Plenum Medical Book Company*, 1986, p 114.

38. Oosawa, Polyelectrolytes, *Marcel Dekker, INC., New York*, 1971; p 23-26.